AFRL-SN-HS-TR- 2002-031

RAMAN ECHO DATA STORAGE IN Pr:YSO CRYSTALS FOR HIGH SPEED IMAGING

Dr. Selim Shahriar
Prof. Shaoul Ezekiel
MASSACHUSETTS INSTITUTE OF TECHNOLOGY
77 Massachusetts Avenue
Cambridge MA 02139

FINAL REPORT: MAY 1997 – MAY 1998

APPROVED FOR PUBLIC RELEASE

AIR FORCE RESEARCH LABORATORY
Sensors Directorate
80 Scott Dr
Hanscom AFB MA 01731-2909

TECHNICAL REPORT

Title: Raman Echo Data Storage in Pr:YSO Crystals for High Speed Imaging

PUBLICATION REVIEW

This report has been reviewed and is approved for publication:

APPROVED:

CHARLES WOODS
AFRL/SNHC
Optoelectronic Technology Branch
Electromagnetics Technology Division

APPROVED:

ROBERT V. McGAHAN
Technical Advisor
Electromagnetics Technology Division

ESC 02-0665

REPORT DOCUMENTATION PAGE

Form Approved
OMB No. 0704-0188

1. AGENCY USE ONLY *(Leave blank)*	2. REPORT DATE	3. REPORT TYPE AND DATES COVERED
	30 June 1998	FINAL 30 May 1997 - 30 May 1998

4. TITLE AND SUBTITLE
Raman Echo Data Storage in Pr:YSO Crystals for High Speed Imaging

5. FUNDING NUMBERS
C - F30602-97-C-0136
PE - 61102F
PR - E-7-7262
PROJ - 2305
TA - D7
WU - PC

6. AUTHOR(S)
Selim Shahrair

7. PERFORMING ORGANIZATION NAME(S) AND ADDRESS(ES)
MIT
77 Massachusetts Avenue
Cambridge, MA 02139

8. PERFORMING ORGANIZATION REPORT NUMBER

9. SPONSORING/MONITORING AGENCY NAME(S) AND ADDRESS(ES)
Charles Woods
AFRL/SNHC
80 Scott Drive
Hanscom AFB, MA 01731-2909

10. SPONSORING/MONITORING AGENCY REPORT NUMBER

11. SUPPLEMENTARY NOTES

12a. DISTRIBUTION AVAILABILITY STATEMENT
Approved for public release; distribution unlimited

12b. DISTRIBUTION CODE
a

13. ABSTRACT *(Maximum 200 words)*

We have demonstrated a ring cavity layer using the gain mechanism of a four-wave mixing process, mediated by two-photon Zeeman coherence resulting from coherent population trapping in a rubidium vapor cell. The cell acts as an amplifying phase conjugate mirror at one corner of the ring cavity. Even though the fundamental process requires non-degeneracy between the probe and the conjugate in the atom's frame, they are degenerate in the laboratory frame, via selection of a moving band of atoms for the gratings. As such, no frequency shifting is necessary in the cavity. The polarization orthogonality of the probe and the conjugate is compensated by an intra-cavity quarter wave plate.

14. SUBJECT TERMS
ring cavity laser

15. NUMBER OF PAGES
14

16. PRICE CODE

17. SECURITY CLASSIFICATION OF REPORT	18. SECURITY CLASSIFICATION OF THIS PAGE	19. SECURITY CLASSIFICATION OF ABSTRACT	20. LIMITATION OF ABSTRACT
UNCLASSIFIED	UNCLASSIFIED	UNCLASSIFIED	SAR

Standard Form 298 (Rev. 2-89) (EG)
Prescribed by ANSI Std. 239.18
Designed using Perform Pro, WHS/DIOR, Oct 94

1. INTRODUCTION

The objective of this project was to explore the feasibility of using Raman echo data storage in Pr:Yso crystals for high speed imaging. To this end, we have made substantial progress. The technical achievements in this project are summarized below.

2. TECHNICAL ACHIEVEMENTS

2.1 Frequency-selective Time-domain Optical Data Storage by Electromagnetically Induced Transparency in a Rare-earth Doped Solid.

Since the proposal[1] and subsequent experimental demonstration of stimulated photon echoes in both vapors[2] and solids,[3] there has been increasing interest in their use for high capacity optical data storage. Much of this interest arises from the large theoretical storage density available in rare-earth doped solids, given by the ratio of optical inhomogeneous to homogeneous widths, which can be in excess of 10^6. However, for rare-earth doped solids, this storage density is generally only available at temperatures below 4 K and decreases rapidly at higher temperatures due to the increase of homogeneous width by phonon interactions. In addition, some of the most widely used rare-earth doped solids require highly frequency-stable lasers to approach theoretical storage densities.[4] To overcome these limitations, we proposed[5] a technique to store optical data using spin coherences excited by coherent population trapping,[6] which in the present context is equivalent to electromagnetically induced transparency (EIT).[7,8] The advantages are that spin coherences tend to have much longer lifetimes than optical coherences at higher temperatures, and that EIT can be made to be insensitive to laser jitter.

In this Letter, we experimentally demonstrate frequency-selective time-domain optical data storage in Pr^{3+}:Y_2SiO_5 (Pr:YSO) using spin echoes excited by EIT. We verify the key prediction that the theoretical storage density does not significantly degrade with increasing crystal temperature up to 6 K. In contrast, at this temperature the theoretical optical storage density determined by the photon echoes is more than an order of magnitude smaller than its value below 4 K (as will be discussed later). We also verify the predicted insensitivity of theoretical storage density to laser frequency jitter.

The optical storage technique described in this Letter is analogous to the frequency-selective stimulated photon echo memory.[1] In this technique, the optical inhomogeneous width is chopped into M accessible channels in the frequency domain, and each channel is used for N-bit data storage in the time domain. Ideally, the Fourier component of each data pulse (and any laser frequency jitter) should be narrower than the assigned channel width. It is easy to show that the maximum storage density, NM, is given by the ratio of optical inhomogeneous to homogeneous widths. The length of the time domain 'write window' is given by the optical transverse relaxation time T_2. In the present experiment, the time-domain portion of the memory utilizes a ground-state spin coherence rather than an optical one. This means that the time domain 'write window' is now given by the spin T_2, which is generally longer than optical T_2, especially at higher temperatures or if there is appreciable laser jitter. Furthermore, if the inhomogeneous

width of the spin transition is equal to or wider than the assigned optical frequency channel, then the theoretical storage density of the new technique is given by the ratio of the optical inhomogeneous width to the spin homogeneous width. This is nearly always larger than the theoretical optical photon echo storage density, especially at high temperatures.

For the detection of frequency-selective stimulated spin echoes excited by EIT, we use enhanced nondegenerate four-wave mixing[8] (NDFWM). The advantage of this technique is to increase echo detection efficiency as shown in a previous paper.[9]

Figure 1 shows energy level diagram of 0.05 at. % Pr doped YSO in which the optical transition frequency of ${}^3H_4 \rightarrow {}^1D_2$ is 605.7 nm. The splittings of the ground-hyperfine states are 10.2 MHz and 17.3 MHz as shown.[10] The time-dependent coherence σ_{12} between the ground states $|1\rangle \leftrightarrow |2\rangle$ in Fig. 1 is created by the two resonant optical fields ω_1 and ω_2 according to the following density matrix equation:

$$d\sigma_{12} / dt = -iD_{13}E_1\sigma_{32}(t)/\hbar + iD_{23}E_2\sigma_{13}(t)/\hbar - \gamma_{12}\sigma_{12}(t), \qquad (1)$$

where D_{ij} is dipole matrix element corresponding to the transition $|i\rangle \rightarrow |j\rangle$, and γ_{12} is the decay rate of σ_{12}. E_1 and E_2 are (slowly varying) pulse amplitudes of the electric fields of the laser beams at ω_1 and ω_2, respectively. Since the ground state coherence term σ_{12} is directly coupled to the optical coherences σ_{13} and σ_{23}, time dependent phenomena can be predicted using perturbation theory as in two level systems.[11]

To probe the ground state coherence, a probe beam ω_P is red-detuned by $\Delta = 1.5$ MHz from the frequency of the beam ω_2, as shown. A repump beam ω_R is used to provide frequency selectivity in the inhomogeneously broadened optical transition as discussed elsewhere.[12] The repump beam is chosen to excite a different transition than the two beams ω_1 and ω_2 to escape from coherent interactions. A stimulated spin echo (rephased coherence σ_{12}) is produced by three resonant Raman pulses each having two frequencies ω_1 and ω_2 and is detected by NDFWM using ω_P to generate the signal beam ω_D which is proportional to the rephased spin coherence.

Figure 2 shows a schematic of the experimental setup. A frequency stabilized cw ring dye laser is pumped by an argon-ion laser. The dye laser has jitter of ~ 1 MHz which is measured using a Febry-Perot spectrum analyzer. We use acousto-optic modulators (AOM) driven by frequency synthesizers to make four coherent laser beams ω_1, ω_2, ω_R, and ω_P from the dye laser output as shown. The laser powers of the beams ω_R, ω_1, ω_2, and ω_P are ~10, 30, 2, and 10 mW, respectively. The use of AOMs makes laser jitter correlated so that laser difference frequencies are stable typically down to sub-kHz. The angle between the beams ω_1 and ω_2 is ~ 60 mrad. The direction of the probe beam is chosen to satisfy Bragg matching, but is not exactly co-propagating with either beams ω_1 or ω_2 (see inset in Fig. 2). The diffracted beam ω_D, which is generated from NDFWM process, satisfies the phase matching condition of $\vec{k}_D = \vec{k}_1 + \vec{k}_2 - \vec{k}_P$. All laser beams are forward propagating, circularly polarized with a quarter wave plate, and focused into the sample (Pr:YSO) by a 40cm focal length lens. The measured beam diameters (1/e in intensity) of the beams are ~150 μm in the crystal. The size of the crystal is 3×6×9 (mm) with its symmetric optical B-axis along the 9 mm direction, and it is mounted inside a cryostat. To pulse the laser beams, rf switches driven by pulse

generators (SRS DG 535 and HP 214 A) are used. The repetition rate of these pulses is 100 Hz. To average the laser jitter noise, thirty diffracted signals are detected by a fast silicon photo-diode (Thorlabs PDA 150) and averaged by a Boxcar averager (SRS 250) with a gate width of 3 μs.

Figure 3 shows the storage of two bits of time-domain optical data by frequency-selective stimulated spin echoes based on EIT. For this data, the crystal temperature is 6 K. Each input pulse is composed of both resonant Raman beams ω_1 and ω_2. The first two input pulses (d and d') are data bits. The second and third input pulses are write (w) and read (r) pulses, respectively. The pulse width of the repump beam is 1 ms (not shown), and immediately precedes the data pulse d. The pulse widths of the data bits (d and d') are 7 μs and 2 μs, respectively, separated by 100 μs. The widths of the write and read pulses (w and r) are 7μs and 5μs, respectively, separated by 1.1 ms which is twice the spin T_2. The time delay between data pulse d' and the write pulse w is 300 μs, which is chosen to be longer than the optical T_2 (111 μs) but shorter than the spin T_2. The probe pulse width is 5μs, and the diffracted signals (30 samples) are averaged by the Boxcar averager. When the input pulses are present, the diffracted signals are off-scale on the chart recorder. As seen in the figure, there are 'two-pulse' echoes just after the write pulse w. The echo signal e is bigger than e' because the data d has a wider area than d'. The stimulated echoes are retrieved by the read pulse r at $t_3 + t_2$ and $t_3 + t_2 - t_1$. Their intensities are comparable with those of the 'two-pulse' echoes. The theoretical storage time is limited by a spin population decay time T_1, which is ~ 100 s in this material[10] but is several hours in Eu:YSO.[13] The storage density of the spin transition is determined by the ratio of spin T_2 to T_2*. This ratio can be made large by applying a magnetic field to slow down the spin T_2,[14] or by using a magnetic field gradient to create additional inhomogeneous broadening.[15]

Figure 4(a) shows the spin T_2 versus temperature. Each spin T_2 is measured from the 'two-pulse' echo intensity (see e in Fig. 3) versus the write pulse delay t_2 with pulses d' and r absent. We varied the write pulse delay time from 100 μs to 900 μs. Fluctuations in figure 4 are caused by laser jitter which affects the observed echo signal intensity. Within the measurement fluctuations, the spin T_2 appears constant up to 6 K.

To infer how the optical T_2 depends on temperature, we simply measure the intensity of 'two-pulse' echo at a fixed write pulse delay t_2 (Fig. 4(b)). The pulse delay t_2 is kept at 400 μs. The echo intensity should be proportional to the square of the optical T_2, since the efficiency of EIT depends on the product of Ω^2 and the optical T_2, where Ω is the rms Rabi frequency for the transitions at ω_1 and ω_2.[16] As we see in Fig. 4(b), the echo intensity decreases exponentially above 4 °K. This implies that the optical T_2 also decreases exponentially as temperature goes up. Beyond 6 K, the signal was too weak to measure the spin T_2 with our low-sensitive photodiode, even though we detected the echoes until the spectral hole-burning pheonema persisted (~ 8 K).

In summary, we observed frequency-selective time-domain optical data storage using EIT excited spin echoes in Pr:YSO at 6 K. The echoes are detected using NDFWM enhanced by EIT. We showed that the write window is determined by the spin T_2 which is much longer than the optical T_2 especially at higher temperature. We also measured the spin T_2 and found it almost constant in the range of 2 - 6 K. In contrast, at temperatures above 4 K, we observed that the optical T_2 decreases exponentially as

References

1. T.W. Mossberg, Opt. Lett. **7**, 77 (1982).
2. N.W. Carlson, L.J. Rothberg, A.G. Yodh, W.R. Babbitt, and T.W. Mossberg, Opt. Lett. **8**, 483 (1983).
3. M.K. Kim and R. Kachru, Opt. Lett. **12**, 593 (1987).
4. X.A. Shen, E. Chiang, and R. Kachru, Opt. Lett. **19**, 1246 (1994).
5. P.R. Hemmer, M.S. Shahriar, B.S. Ham, M.K. Kim, Y. Rozhdestvensky, Mol. Cryst. Liq. Cryst. **291**, 287 (1996).
6. G. Alzetta, A. Gozzini, L. Moi, and G. Orriols, Nuovo Cimento B **36**, 5 (1976); H.R. Gray, R.M. Whitley, and C.R. Stroud, Jr., Opt. Lett. **3**, 218 (1978).
7. K.-J. Boller, A. Imamoglu, and S.E. Harris, Phys. Rev. Lett. **66**, 2593 (1991); B.S. Ham, P.R. Hemmer, and M.S. Shahriar, Opt. Comm. (to be published)
8. S.E. Harris, J.E. Field, and A. Imamoglu, Phys. Rev. Lett. **64**, 1107 (1990); B.S. Ham, M.S. Shahriar, and P.R. Hemmer, Opt. Lett. **22**, 1138 (1997).
9. B.S. Ham, M.K. Kim, P.R. Hemmer, and M.S. Shahriar (submitted).
10. K. Holliday, M. Croci, E. Vauthey, and U.P. Wild, Phys. Rev. B. **47**, 14741 (1993).
11. M. Mitsunaga and R.G. Brewer, Phys. Rev. A**32**, 1605 (1985).
12. B.S. Ham, M.K. Kim, P.R. Hemmer, and M.S. Shahriar (to be submitted).
13. R. Yano, M. Nitsunaga, and N. Uesugi, Opt. Lett. **16**, 1884 (1991).
14. R.M. Macfarlane, C.S. Yannoni, and R.M. Shelby, Opt. Comm. **32**, 101 (1980).
15. P.R. Hemmer, K.Z. Cheng, J. Kierstead, M.S. Shahriar, and M.K. Kim, Opt. Lett. **19**, 296 (1994).
16. P.R. Hemmer, M.S. Shahriar, V.D. Natoli, and S. Ezekiel, J. Opt. Soc. Am. B **6**, 1519 (1989).

temperature goes up. Therefore these results demonstrate the potential of higher capacity optical data storage than by conventional photon echo methods in rare-earth doped solids at high temperatures.

Figure Captions:

FIG. 1. Energy level diagram of Pr:YSO.
FIG. 2. Schematic of the experimental setup for frequency-selective time-domain stimulated spin echo by EIT; AOM, Acousto-optic modulator; BOX, Boxcar averager; BS, Beam Splitter; CR, Chart Recorder; L, Lens; M, Mirror; OSC, Oscilloscope; PA, rf power amplifier; PD, Photo Diode; PG, pulse generator; S, rf Switch; SC, Screen.
FIG. 3. Two-bit optical data storage by frequency-selective time-domain stimulated spin echo based on EIT at 6 K: d and d', data; e and e', echoes.
FIG. 4. (a) Spin T_2 versus temperature. (b) Inferred optical T_2 versus temperature.

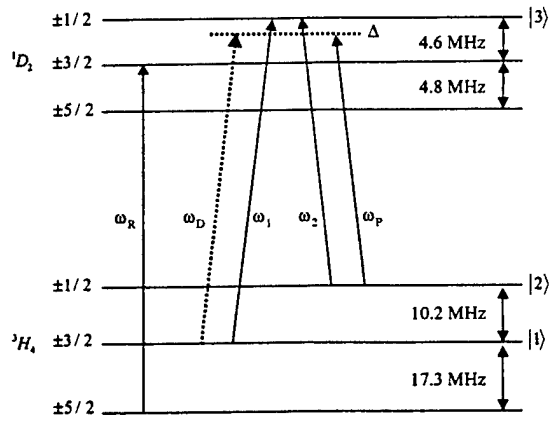

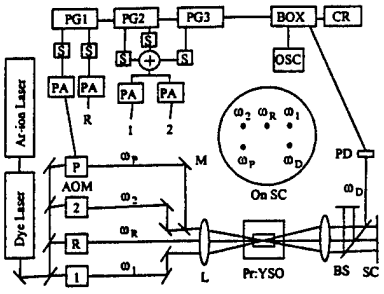
PG1
PG2
PG3
BOX
CR
OSC
S
PA
R
1
2
Ar-ion Laser
Dye Laser
P
AOM
2
R
1
M
L
On SC
Pr:YSO
PD
BS
SC

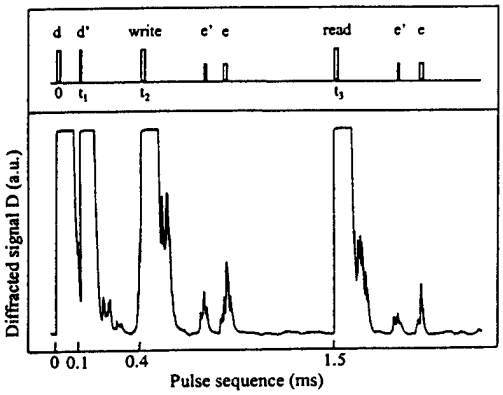
d
d'
write
e'
e
read
e'
e
0
t1
t2
t3
Diffracted signal D (a.u.)
0
0.1
0.4
1.5
Pulse sequence (ms)

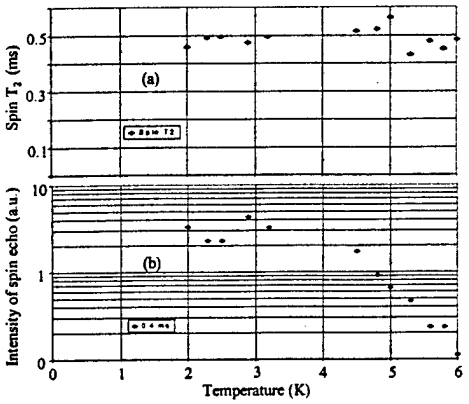
Spin T_2 (ms)
0.5
0.3
0.1
(a)
10
1
0
(b)
Intensity of spin echo (a.u.)
0
1
2
3
4
5
6
Temperature (K)

2.2 Observation of Electromagnetically Induced Transparency Above the Spectral-Hole-Burning Temperature Range

As information technology develops, not only large-capacity storage but also high-speed information processing is important for mass data communications. Recently, spectral hole-burning materials have attracted much attention because of potential applications in mass optical data storage, fast optical switches, and computing elements such as a dynamic random access memory module. For example, the usefulness of the hole-burning materials for high-density storage[1] and high-speed optical switches[2] has been already demonstrated using photon echoes.

In the spectral hole-burning media, the storage capacity is significantly increased by wavelength multiplexing using the large ratio of inhomogeneous to homogenous width for the optical transition. This wavelength multiplexing does not suffer from Bragg degeneracy caused cross-talk,[3] which limits storage capacity in volume holographic memories. That is because adjacent spectral holes are composed of different subsets of atoms, molecules, or ions.[4] In rare earth doped solids, the storage densities are $\sim 10^6$. This large storage density, however, is only available near liquid helium temperatures, because the optical homogenous width rapidly increases at higher temperatures due to phonon interactions.

Recently a spin echo memory excited by resonant Raman pulses has demonstrated the potential to overcome the temperature restrictions in the photon echo-based memories.[5] In the resonant Raman excited spin echo memory, it was shown that the spin coherence time T_2 (reciprocal of the homogeneous width) replaces the optical T_2 for the length of the write window. Thus, under ideal conditions, the memory density is determined by the ratio of the optical inhomogeneous width to spin, rather than the optical, homogeneous width. This is especially important for higher temperature applications, because the spin homogeneous width is less temperature sensitive. For example, we demonstrated the narrower and temperature insensitive spin homogeneous width in Pr^{3+} doped Y_2SiO_5 (Pr:YSO) up to 6K.[5]

For the efficient Raman excited spin echoes, electromagnetically induced transparency[6] (EIT) is an essential condition. In a three-level system interacting with Raman fields, EIT is caused by destructive quantum interference, so that the optically thick medium can be transparent. Recent demonstrations of EIT[7,8] and resonant Raman excited spin-echoes[5,9] in solids, however, still required near liquid helium temperatures. Here, we present an experimental observation of EIT in Pr:YSO at temperatures up to 15K well beyond the spectral hole-burning temperature. We show that the probe transmission increases by a factor of exp(1.4) at 12K.

Our system consists of 0.05 at. % Pr doped YSO in which Pr^{3+} substitutes Y^{3+}. For this work, the relevant optical transition is ${}^3H_4 \rightarrow {}^1D_2$, which has a frequency of ~ 606 nm. The inhomogeneous width of the optical transition is ~4 GHz at 1.4 K. The optical population decay time T_1 and transverse decay time T_2 are 164 μs and 111 μs, respectively at 1.4 K.[10] The ground (${}^3H_4$) and excited (${}^1D_2$) states have three degenerate hyperfine states, respectively. The splittings between the ground-hyperfine states are 10.2

MHz ($\pm 1/2 \leftrightarrow \pm 3/2$), 17.3 MHz ($\pm 3/2 \leftrightarrow \pm 5/2$), and 27.5 MHz ($\pm 1/2 \leftrightarrow \pm 5/2$).[10] The ground state spin decay times T_1 and T_2 are ~100 s[11] and 500 ms,[5] respectively, at 6 K for the 10.2 MHz transition. The spin inhomogeneous width for the 27.5 MHz transition is 80 kHz at 1.6K.[11]

Fig. 1 shows a schematic of the experimental setup. We use a frequency stabilized ring dye laser. The dye laser frequency jitter is about 2 MHz. For the resonant Raman transition, we excited the $^3H_4$ ($\pm 1/2$) $\rightarrow$ $^1D_2$ ($\pm 3/2$) transition with a coupling laser and the $^3H_4$ ($\pm 5/2$) $\rightarrow$ $^1D_2$ ($\pm 3/2$) transition with a probe laser. The coupling and probe fields are upshifted by 72.5 MHz and 100 MHz from the laser frequency, respectively. These fields are generated using acousto-optic modulators (AO) driven by frequency synthesizers (PTS 160). The probe field is fixed at resonance, while the coupling field is scanned across its resonance. The two laser beams are circularly polarized with a quarter wave plate and focused into the sample by a 25-cm focal length lens. The diameter (1/e in intensity) of the coupling laser beam is about ~ 50 μm in the crystal. The coupling laser intensity is varied up to a maximum of ~1.5 kW/cm^2. To produce laser pulses, we used rf switches driven by pulse generators. The pulse width is fixed at 50μs. A Boxcar averager averages 30 samples of the probe signal. The pulse repetition rate is 50 Hz. The angle between the coupling and probe fields is about 100 mrad. The spectral hole-burning crystal of Pr:YSO is inside a cryostat and its temperature can be varied. The size of the crystal is 3 mm×6 mm ×1 mm. Its optical B-axis is along the 1-mm length, and laser propagation direction is almost parallel to the optical axis.

Fig. 2 shows the probe absorption as a function of temperature. In Fig. 2, the coupling laser is blocked, and the probe intensity is adjusted not to saturate (over the temperature of the spectral hole burning). The power of the probe beam is 60 μW. Below ~8 K, the sample is nearly transparent to the probe because of spectral hole burning. The probe transmission rapidly decreases to ~10% at 10K. The minimum transmission of the probe is 4% at 20K. This high probe absorption continues up to ~25K and then gradually decreases. From the data in Fig. 2, the absorption coefficient α is calculated to be ~30/cm at the temperatures 12K - 20 K.

Fig. 3 shows the probe transmission versus the coupling laser detuning at 12K. The maximum coupling laser intensity is 1.2 kW/cm^2 in the crystal. At line center (Δ=0) of the coupling laser transition, the probe transmission is increased from 5% to 20 %, a factor of exp(1.4). The FWHM of the probe transmission increase is ~ 2.2 MHz. This width is much narrower than the optical homogeneous width at this temperature, which is deduced to be larger than 10.2 MHz, based on the assumption that the spectral hole-burning disappears when the the optical homogeneous width is larger than the ground state hyperfine splitting. This sub-natural linewidth in the probe spectrum (Fig. 3) is taken as evidence of EIT. Here, the efficiency of EIT is limited by available laser power. In previous work (Ref. 7), more efficient EIT was seen for lower coupling laser intensity, but the temperature was much lower. This is because the EIT efficiency is inversely proportional to the homogeneous width of the optical transition, which is broader at high temperatures.

In Fig. 4, we keep the temperature at 10 K, which gives partial spectral hole burning. Initially, the probe absorption is suppressed owing to EIT (see Fig. 3). When

the coupling laser beam is switched off (at t=0 in Fig. 4), the probe beam absorption first increases and then gradually decreases. The absorption increase at t=0 is due to loss of EIT; coherently trapped ions begin to absorb the photons. The absorption decrease afterward is because of the spectral hole burning. The spectral hole-burning saturation time depends on the strength of the probe.

Fig. 5 shows the probe transparency versus the coupling laser intensity. The temperature is fixed at 12 K. As expected, the probe transparency increases as the coupling laser intensity increases. The probe transparency increase is proportional to the square root of the coupling laser intensity. The coupling intensity axis is a log scale. For the data, the probe transparency is determined by the probe transmission change when the coupling laser is switched on.

In Fig. 6, we measured the probe transparency as a function of temperature with a fixed intensity of the coupling laser. As expected, the probe transparency decreases as the temperature increases. This is because the optical homogeneous width is broadened as the temperature increases, so that the EIT efficiency decreases. Over 15 K, we could not detect the EIT effect with our maximum coupling laser intensity of ~1.2 kW/cm^2.

To summarize, we experimentally observed EIT in an optically thick, spectral hole-burning solid of Pr:YSO at higher temperatures than needed for spectral hole-burning. This demonstration is the first step toward implementation of high-density, high-speed optical memories based on resonant Raman excited spin echoes. The Raman excited spin echo memory can achieve the higher temperature memory applications, because the spin homogeneous width is less temperature sensitive than the optical width.

Figure Captions

FIG. 1. Schematic of the experimental setup.

FIG. 2. Probe transmission versus temperature. The probe laser power is 60 μW.

FIG. 3. Probe transmission versus coupling laser detuning at 12K.

FIG. 4. Probe transmission versus time. At t=0, the coupling laser is off.

FIG. 5. Probe transparency versus coupling laser intensity.

FIG. 6. Probe transparency versus temperature for fixed coupling laser intensity.

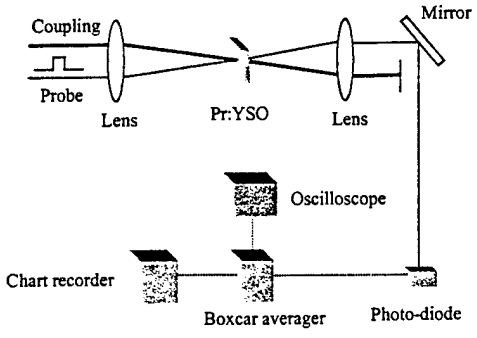

Figure 1.

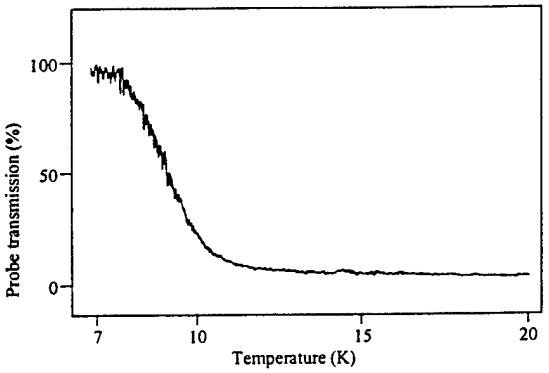

Figure 2.

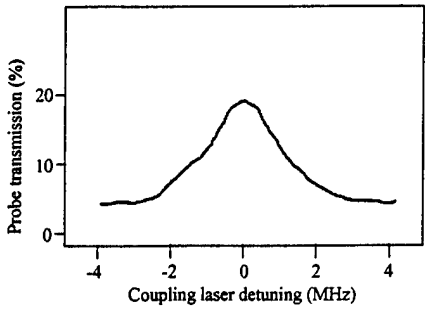

Figure 3.

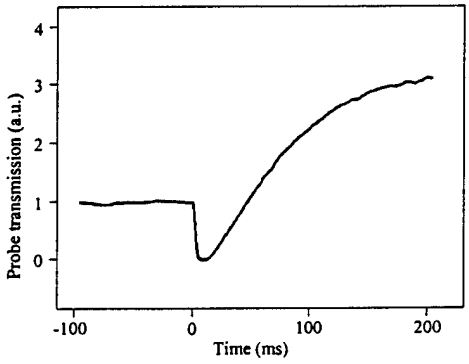

Figure 4.

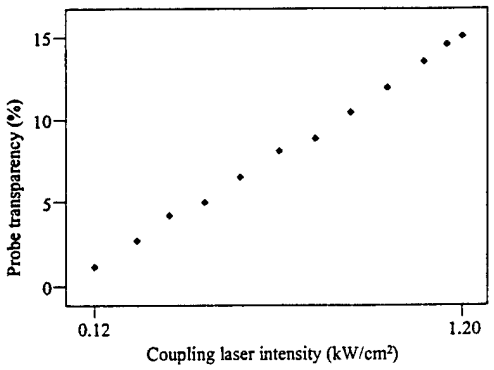

Figure 5.

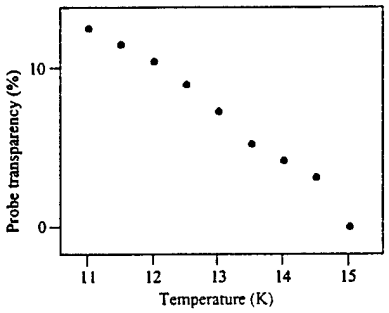

Figure 6.

References

1. H. Lin, T. Wang, and T. W. Mossberg, "Demonstration of 8-Gbit/in.2 areal storage density based on swept-carrier frequency-selective optical memory," Opt. Lett. **20**, 1658 (1995).
2. X. A. Shen and R. Kachru, "Optical header recognition by spectroholographic filtering," Opt. Lett. **20**, 2508 (1995).
3. D. Psaltis, D. Brady, X.-G. Gu, and S. Lin, "Holography i artificial neural networks," Nature **343**, 325 (1990); A. Chiou, "Anisotropic corss talk in an optical interconnection by using a self-pumped phase-conjugate mirror at the Fourier plane," Opt. Lett. **17**, 1018 (1992).
4. U. P. Wild, S. E. Bucher, and F. A. Burkhalter, "Hole burning, Stark effect, and data storage," Appl. Opt. **24**, 1526 (1985).
5. B. S. Ham, M. S. Shahriar, M. K. Kim, and P. R. Hemmer, "Frequency-selective time-domain optical data storage by electromagnetically induced transparency in a rare-earth doped solid," Opt. Lett. **22**, 1849 (1997).
6. K. J. Boller, A. Imamoglu, and S. E. Harris, "Observation of electromagnetically induced transparency," Phys. Rev. Lett. **66**, 2593 (1991).
7. Y. Zhao, C. Wu, B. S. Ham, M. K. Kim, and E. Awad, "Microwave induced transparency in ruby," Phys. Rev. Lett. **79**, 641 (1997); B. S. Ham, P. R. Hemmer, and M. S. Shahriar, "Efficient electromagnetically induced transparency in a rare-earth doped crystal," Opt. Commun. **144**, 227 (1997).
8. B. S. Ham, M. S. Shahriar, P. R. Hemmer, "Enhanced nondegenerate four-wave mixing owing to electromagnetically induced transparency in a spectral hole-burning crystal," Opt. Lett. **22**, 1138 (1997).
9. B. S. Ham, M. S. Shahriar, M. K. Kim, P. R. Hemmer, "Spin coherence excitation and rephasing with optically shelved atoms," Phys. Rev. **B 58**, Rapid Comm. (In press).
10. R. W. Equall, R. L. Cone, and R. M. Macfarlane, "Homogeneous broadening and hyperfine structure of optical transitions in Pr3+:Y2SiO5," Phys. Rev. **B 52**, 3963 (1995).
11. K. Holliday, M. Croci, E. Vauthey, and U. P. Wild, "Spectral hole burning and holography in an Y2SiO5:Pr3+ crystal," Phys. Rev. **B 47**, 14741 (1993).